ADVANCED MATERIALS
www.advmat.de

Empowering CO_2 Eco-Refrigeration With Colossal Breathing-Caloric-Like Effects in MOF-508b

María Gelpi, Javier García-Ben, Sabina Rodríguez-Hermida, Jorge López-Beceiro, Ramón Artiaga, Álvaro Baaliña, Manuel Romero-Gómez, Javier Romero-Gómez, Sonia Zaragoza, Jorge Salgado-Beceiro, Julian Walker, Charles James McMonagle, Socorro Castro-García, Manuel Sánchez-Andújar, María Antonia Señarís-Rodríguez, and Juan Manuel Bermúdez-García**

In loving memory of Juan Manuel Bermúdez Rubí, who always transmitted his passion and knowledge about mechanical designs and inventions with joy

Today, ≈20% of the electric consumption is devoted to refrigeration; while, ≈50% of the final energy is dedicated to heating applications. In this scenario, many cooling devices and heat-pumps are transitioning toward the use of CO_2 as an eco-friendly refrigerant, favoring carbon circular economy. Nevertheless, CO_2 still has some limitations, such as large operating pressures (70–150 bar) and a critical point at 31 °C, which compromises efficiency and increases technological complexity. Very recently, an innovative breathing-caloric mechanism in the MIL-53(Al) compound is reported, which implies gas adsorption under CO_2 pressurization boosted by structural transitions and which overcomes the limitations of stand-alone CO_2. Here, the breathing-caloric-like effects of MOF-508b are reported, surpassing by 40% those of MIL-53(Al). Moreover, the first thermometry device operating at room temperature and under the application of only 26 bar of CO_2 is presented. Under those conditions, this material presents values of $\Delta T \approx$ 30 K, reaching heating temperatures of 56 °C and cooling temperatures of −10 °C, which are already useful for space heating, air-conditioning, food refrigeration, and freezing applications.

1. Introduction

Decarbonization of heating and cooling sectors is one of the main challenges in the international agenda,[1] directly related to the United Nations Sustainable Development Goals.[2] Refrigeration already accounts for ≈20% of the electric energy consumption,[3] meanwhile heating global energy demand is as large as 50%.[4] Further, in some cases such as in the residential sector, the refrigeration energy demand is expected to surpass that required for heating by the year 2050.[5] Therefore, more efficient technologies will be required in the near future.

In addition, the most extended commercial cooling systems are based on vapor compression of refrigerant gases. In addition, most of these gases are fluorinated compounds with significantly large global warming potentials, GWP (for example, two of the most common refrigerants exhibit

M. Gelpi, J. García-Ben, S. Castro-García, M. Sánchez-Andújar, M. A. Señarís-Rodríguez, J. M. Bermúdez-García
QuiMolMat Group
Department of Chemistry
Faculty of Science and Centro Interdisciplinar de Química e Bioloxía (CICA)
University of A Coruna
Zapateira, A Coruña 15071, Spain
E-mail: m.senaris.rodriguez@udc.es; j.bermudez@udc.es

The ORCID identification number(s) for the author(s) of this article can be found under https://doi.org/10.1002/adma.202310499

DOI: 10.1002/adma.202310499

S. Rodríguez-Hermida
Research Support Services
University of A Coruna
A Coruña 15071, Spain

J. López-Beceiro, R. Artiaga
CITENI-Proterm Group
Ferrol Industrial Campus
Campus de Esteiro
University of A Coruna
Ferrol 15403, Spain

Á. Baaliña, M. Romero-Gómez, J. Romero-Gómez
Energy Engineering Research Group
Department of Nautical Sciences and Marine Engineering (ETSNM)
University Institute of Maritime Studies
University of A Coruna
Paseo de Ronda, 51, A Coruña 15011, Spain

S. Zaragoza
CITENI, Ferrol Industrial Campus
University of A Coruna
Ferrol, A Coruña 15403, Spain

values of GWP(R134a) = 1430 or GWP(R32) = 677). In that regard, the international Kigali Agreement and the European F-gas regulation (EU 517/2014) are progressively phasing out up to 80% of those gases by the year 2050. Therefore, natural refrigerants such as hydrocarbons (HCs), ammonia (NH_3), or carbon dioxide (CO_2) are proposed as greener alternatives. However, HCs are flammable compounds strictly controlled by the ATEX directive (2014/34/EU) and ammonia is toxic and corrosive; while, CO_2 does not share these hazards.

In parallel, and accelerated by the climatic crisis, the international community is also seeking for new technologies that can incorporate CO_2 in the value chain, favor the carbon circular economy, and avoid these hazardous emissions.[6]

In that regard, the sector of heating, ventilation, air-conditioning and refrigeration (HVAC&R) is currently transitioning toward the use of the vapor compression of CO_2 as an eco-friendly refrigerant, labeled as R-744.[7] This refrigerant gas presents important advantages compared to most of the other commercial refrigerants for vapor compression systems, namely: i) it presents a global warming potential (GWP) of only 1, while common refrigerants have a GWP value of several hundreds or thousands; ii) it is economically affordable and widely available, and iii) it is not toxic, corrosive or flammable. Nevertheless, this refrigerant requires relatively larger operating pressures of 70–150 bar (in contrast to the ≈10 bar required for the rest of refrigerant gases), and it is difficult to operate in warm climates above 31 °C due to the presence of a critical point.[8]

Alternatively, the scientific community is exploring the combination of CO_2 with solid adsorption materials to exploit the adsorption/desorption enthalpies as a heating and/or cooling mechanism.[9,10] In this context, most of the studied adsorption materials for CO_2 adsorption refrigeration/heating applications are carbons, zeolites, and—in a few recent reports—also, porous metal–organic frameworks (MOFs). Nevertheless, when comparing with vapor compression, adsorption technologies require the continuous regeneration of the adsorbents through heating and/or high vacuum,[9,10] which adds complexity to the systems and decreases their efficiency.[11] On the other hand, all-solid-state barocaloric materials are becoming a promising alternative for emissions-free refrigeration and heating applications. Barocaloric materials are solid compounds that present thermal changes related to pressure-induced solid-to-solid phase transitions and have experienced an accelerated development in the last decade.[12–18] Nevertheless, most of the barocaloric materials still operate at very large pressures above 1000 bar and show thermal changes whose values are still far from those of refrigerant gases, limitations which have hindered their commercial implementation up to date.[12,19]

In 2021, metal–organic frameworks (MOFs) with breathing transitions (structural phase transitions between two crystalline phases with different pore size upon uptake/release of gas[20,21]) were proposed as potential barocaloric materials to explore in the future.[22,23] Breathing MOFs belong to the singular class of flexible MOFs, which are known to display structural changes under different external stimuli (such as temperature, mechanical pressure or gas adsorption among others).[24–26]

In that regard, and even if coming from a different research field, previous studies on MOFs have already reported large thermal changes upon gas adsorption, a feature which was considered a major drawback for their use in gas adsorption and storage applications.[27,28] So, in that case, most efforts have been focused on trying to avoid and/or minimize those thermal changes.[27,28]

In 2022, members of our team reported the first experimental work on pressure-induced caloric effects in breathing MOFs of interest for heating and cooling applications. We discovered that MIL-53(Al) (MIL = Matériaux de l'Institut Lavoisier), when pressurized with CO_2, presented very large pressure-induced caloric effects related to its breathing transition, which combines thermal changes from both the gas adsorption process and the solid-to-solid structural transition. This dual caloric mechanism arising from the breathing transition was coined as "breathing-caloric effect."[29] Despite the fact that this was the first report on breathing-caloric effects, the chosen compound, MIL-53(Al) already presented very large thermal changes ($\Delta H_{\text{MIL-53(Al)}} \approx 93$ kJ kg^{-1}, $\Delta S_{\text{MIL-53(Al)}} \approx 311$ J K^{-1} kg^{-1})[29] similar to those of pure CO_2 as stand-alone vapor compression refrigerant ($\Delta H_{CO2} \approx 120$ kJ kg^{-1}, $\Delta S_{CO2} \approx 401$ J K^{-1} kg^{-1}).[30] In addition, this material required a much lower operating pressure of only 16 bar, compared with the 70–150 bar for the pure CO_2 (or with the 1000 bar of barocalorics), and it could also operate up to 60 °C (well above the CO_2 critical point of 31 °C). Therefore, this new refrigeration mechanism opened new opportunities for designing more sustainable refrigeration technologies. However, there are still many challenges and open questions to be solved before their technological implementation can take place. Among others, it is necessary to measure the value of the adiabatic temperature change that can be reached by this breathing-caloric effect.

As a decisive step forward in the field, in this work, we present a promising new material for breathing-caloric based refrigeration and heating (already surpassing the MIL-53(Al)); while, we also show direct evidence of its adiabatic temperature change upon CO_2 cyclic pressurization.

For this study, we select the MOF-508b of general formula $[Zn_2(bdc)_2(bpy)]$ (bdc = 1,4-benzenedicarboxylate, bpy = 4,4′-bipyridine), initially prepared by Chen et al., and previously studied for alkanes selective separation[31] and for CO_2 separation from gas mixtures.[32]

We choose this compound because it presents two consecutive solid–solid transitions that, in principle, could maximize the resulting pressure-induced thermal changes. Further, the reported preliminary single-crystal X-ray diffraction analysis,[33] even if performed only at three different pressures, suggests that the MOF-508b could have a much lower volume change than MIL-53(Al). This, in turn, would generate less mechanical strain.

J. Salgado-Beceiro
SINTEF Energy Research
Trondheim 7034, Norway
J. Walker
Department of Materials Science and Engineering
Norwegian University of Science and Technology
Trondheim 7491, Norway
C. J. McMonagle
Swiss–Norwegian Beamlines
European Synchrotron Radiation Facility
Grenoble 38043, France

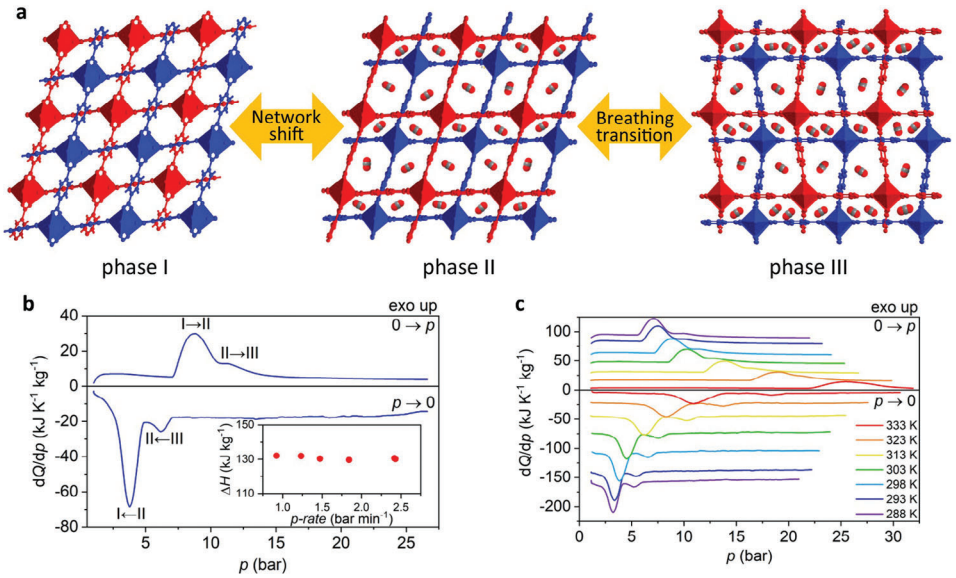

Figure 1. a) Representation of the main modifications of the crystal structure across the solid-solid phase transitions related to the observed thermal transitions. Note: the different interpenetrated subnetworks are represented in red and blue; and CO_2 molecules are randomly placed to illustrate the gas adsorption. Crystal structures are represented from reported CIF files.[33] b) Calorimetric curve obtained by VP-DSC under isothermal conditions at 298 K and under pressurization ($0 \rightarrow p$) and depressurization ($p \rightarrow 0$) rate of 2.5 bar min^{-1}. Inset: enthalpy change (ΔH) of the full thermal process as a function of pressurization rate. c) VP-DSC curves represented for different isothermal conditions from 288 up to 333 K for pressurization ($0 \rightarrow p$) and depressurization rates of 2.5 bar min^{-1}. Note: curves have been vertically displaced for facilitating visualization.

From the structural point of view, this MOF-508b consists of two interpenetrated networks, each one showing hexahedron-like cavities partially blocked with metallic nodes from the corners of the other subnetwork (**Figure 1a**). These metallic nodes are formed by Zn paddle-wheels linked by bdc ligands forming 2D layers that are interconnected by bpy pillars, which leads to the final 3D structure (Figure S1, Supporting Information).

As reported by Bhatt et al.,[33] the first transition is due to a displacement of the interpenetrated networks, while the second one is a breathing transition (Figure 1a).[28] These authors also studied, from the fundamental point of view, the enthalpy changes of adsorption of CO_2 in the MOF-508b at discrete pressures by using variable-pressure differential scanning calorimetry (VP-DSC) at a slow-enough rate to reach quasi-equilibrium state.[28,33]

In the present work, we delve into the calorimetric and thermometric studies using significantly faster pressurizing rates, which are desirable to reduce the time for reaching the target temperature in future heating and cooling devices.

In this manner, we are able to calculate the MOF-508b breathing-caloric-like effects and compare these thermal changes with those of selected vapor-compression and barocaloric refrigerants, as well as with emerging pressure-induced adsorption CO_2 systems. As later discussed, the observed thermal changes in MOF-508b surpass by 40% those of MIL-53(Al), while exhibiting additional advantages for future integration in devices. We also present the first thermometry device (up to our knowledge) designed to directly demonstrate the cooling and heating effects in breathing-caloric materials (and also in related barocaloric materials) upon CO_2 pressurization.

In the specific case of MOF-508b, at room temperature and under the application of only 26 bar of CO_2, we are able to obtain heating temperatures of up to 56 °C and cooling temperatures down to −10 °C. It should be highlighted that these temperatures are already useful for space heating, air-conditioning, food refrigeration, and freezing applications.

2. Results and Discussion

2.1. Basic Characterization

Following the procedure described in the Experimental Section, MOF-508b is obtained with a 70% yield and without impurities according to powder XRD (Figure S2, Supporting Information). Moreover, we also find that the porous structure is in agreement with the literature,[31] showing a BET surface area of 609 m^2 g^{-1} and a Langmuir surface area of 756 m^2 g^{-1} (Figure S3, SI), while the total pore volume and micropore volume values are ≈0.31 cm^3 g^{-1} and ≈0.11 cm^3 g^{-1}, respectively (see Figure S4, Supporting Information for pore size distribution). In the same line, we observe a particle size distribution of 0.5–14 μm (Figures S5 and S6, Supporting Information).

2.2. Pressure-Induced Caloric Effects Obtained by VP-DSC

We have evaluated the pressure-induced caloric effects in the MOF-508b material by using direct variable-pressure differential scanning calorimetry (VP-DSC), studies which are in general very scarce in the literature due to instrumental complexity.

Upon CO_2 pressurization at room temperature (298 K), the MOF-508b material exhibits a very large exothermic peak followed by a smaller exothermic shoulder at higher pressures (Figure 1b). These thermal transitions seem fully reversible upon depressurization.

The observed thermal transitions can be attributed to the reported structural transitions between three different polymorphs (labeled from lower to higher pressure as phases I, II, and III).[33] These results are in agreement with the thermal studies performed by Bhatt et al.,[33] even if here, we use a pressurization/depressurization rate ten times faster.

Under these latter rates, more adequate for refrigeration and heating cycles, our analysis indicates that upon pressurization, the two transitions, between phases I → II and II → III, occur at $p_{t(0\rightarrow p)} \approx 8.8$ bar and ≈11.2 bar, respectively (Figure 1b). Both transitions are relatively wide and partially overlap. Meanwhile, upon depressurization, the transitions take place at $p_{t(p\rightarrow 0)} \approx 3.8$ bar (II → I) and ≈6.2 bar (III → II). It should be noted that these transitions are much sharper and better resolved than the pressurization ones, which might indicate that the depressurization process is faster.

The thermal changes are calculated by integrating the whole area under the curve in the pressure range from 1 to 26 bar, once the blank baseline is subtracted (see the Experimental Section) to avoid any extra contribution coming from CO_2 gas compression. In that manner, the obtained values are as large as $|\Delta H|_{0\rightarrow p} \approx$ 130.6 kJ kg^{-1} and $|\Delta S|_{0\rightarrow p} \approx$ 438.0 J K^{-1} kg^{-1}, and $|\Delta H|_{p\rightarrow 0} \approx$ 144.3 kJ kg^{-1} and $|\Delta S|_{p\rightarrow 0} \approx$ 484.0 J K^{-1} kg^{-1}. As will be discussed later, these thermal changes (normalized per mass of MOF-508b) arise from the combination of CO_2 adsorption/desorption and solid–solid phase transitions.

Regarding the material cyclability, we have observed that, after two conditioning cycles, the MOF-508b exhibits a stationary and fully reproducible performance over time (Figures S7 and S8, Supporting Information). This is an advantage regarding the thermal activation requirement of MIL-53(Al), given that in the case of MOF-508b, no extra heating source is necessary.

Remarkably, the thermal changes also remain independent from the pressurization rate from 0.9 to 2.5 bar min^{-1} (Figure 1b inset).

On the other hand, when we perform a slower point-by-point calorimetric analysis (Figure S9, Supporting Information), those thermal changes slightly increase around ≈ 17% ($|\Delta H|_{0\rightarrow p} \approx$ 153.3 kJ kg^{-1}, $|\Delta S|_{0\rightarrow p} \approx$ 514.3 J K^{-1} kg^{-1}, $|\Delta H|_{p\rightarrow 0} \approx$ 160.8 kJ kg^{-1}, and $|\Delta S|_{p\rightarrow 0} \approx$ 593.3 J K^{-1} kg^{-1}), which can be attributed to the longer analysis time that would allow to reach the complete thermodynamic equilibrium in each step. In any case, for practical heating and cooling applications, faster pressurization rates are preferred, conditions in which our material can still maintain over 80% of the total thermal changes.

It should also be noted that the compound remains stable up to 650 K (Figure S10, Supporting Information), confirming its robustness toward thermal degradation.

To further evaluate the potential applicability of this material under different climates and/or seasons, we perform VP-DSC analysis at different temperatures from 288 to 333 K, trying to cover mild to extremely hot ambient temperatures for daily life applications (Figure 1c). The observed results indicate that the thermal changes remain almost invariant from 288 to 303 K. For higher temperatures, between 313 and 333 K, the thermal changes noticeably decrease; although, they still maintain ≈60% of the original—and remarkably large—value (Figure S11, Supporting Information). In addition, it is observed that the transition pressure increases only slightly with the operating temperature; so that, only 30 bar is required for temperatures as high as 333 K. This pressure value is still much smaller than that required for stand-alone CO_2 cooling systems.

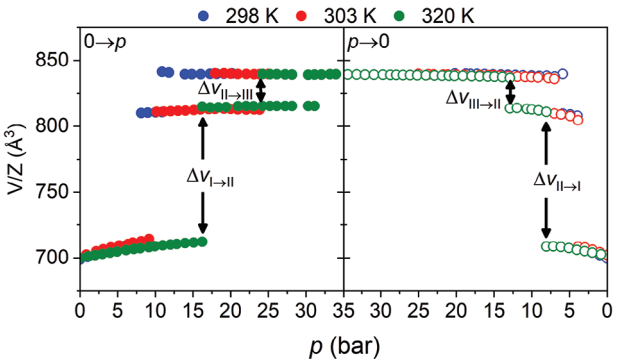

Figure 2. Volume evolution for MOF-508b upon pressurization (full circles) and depressurization (open circles) of CO_2 at different temperatures from 298 K to 320 K. Note: black arrows indicate sharp volume changes at the structural transition pressures.

2.3. Structural Effects and Microscopic Origin of the Observed Caloric Effects

As previously mentioned, the observed pressure-induced caloric transitions in MOF-508b can be associated with two types of structural phase transitions.[33] The first pressure-induced phase transition (I ↔ II at lower pressure) is provoked by a displacement of the two subnetworks (process somehow similar to a breathing-like transition), which opens the MOF's pores to facilitate CO_2 adsorption (see Figure 1a). Meanwhile, the second pressure-induced phase transition (II ↔ III at higher pressure) is a pure breathing effect in which the ligands rotate to further expand the volume of the pores, which in turn, allows to adsorb more CO_2 molecules.[28,33]

In order to deepen further into this structural behavior, we monitor in detail, and for the first time, these transitions by variable-pressure synchrotron powder X-ray diffraction (VP-SPXRD) at different temperatures (Figures S12–S14, Supporting Information). A first interesting result is that the lattice volume evolution as a function of pressure is practically temperature-independent in the whole operating range (**Figure 2**). As for its variation upon CO_2 pressurization, the larger volume increase takes place at each of the structural phase transitions, with expansions of 14.4% (I → II) and 3.8% (II → III), changes that are fully reversible when depressurizing. Therefore, the larger volume increase of the first transition will allow for a larger amount of CO_2 adsorption, which explains the larger thermal signal observed by VP-DSC.

It should be noted that the volume change of MOF-508b upon CO_2 pressurization/depressurization is much smaller than that of the first (and so far, only) breathing-caloric material, the MIL-53(Al), which presents a volume change of ≈40%.[34] This is a very relevant result for technological applications because the use of MOF-508b will imply a much lower mechanical strain on the walls and pipes of a working device. Further, the volume remains almost constant in the regions without transitions, which would also minimize these strains.

Regarding the microscopic origin of the observed caloric effects, it should be noted that this compound displays two types of thermal changes: one related to the adsorption/desorption of CO_2 molecules inside the pores, and a second one related to the volume change observed in this work for the structural transitions.

Rather recent VP-DSC studies at low pressurization rates and quasi-equilibrium state were able to partially separate these two processes, which were in fact found to be opposite in sign.[28] Upon pressurization, the structural transitions were endothermic, while the CO_2 adsorption was exothermic. In addition, the contrary occurred upon depressurization. In addition, the enthalpy change of adsorption/desorption processes seemed to be much larger than those thermal changes attributed to the structural transitions; although, the partial overlapping of both contributions hindered a proper quantification.[28]

In our studies at fast pressurization rates of interest for caloric cooling and heating, we find that both processes take place simultaneously and cannot be separated. However, as our obtained caloric effect upon pressurization is exothermic, we can deduce that the adsorption/desorption effect is prevalent over the volume change, which is similar to the case of MIL-53(Al).[29] In fact, as observed in Figure 1b, the first transition is more energetic than the second one, which can be attributed to a larger volume change (Figure 2) that allows the adsorption of a larger amount of CO_2. This is in agreement with the literature, where adsorption studies corroborate a larger CO_2 uptake across the first transition.[28,33] On the other hand, the decrease of the caloric effects with temperature (Figure 1c) can be explained by the temperature dependence of CO_2 adsorption as described in the literature.[28,33] In these reported studies, there is an adsorption saturation for pressures above 20 bar with a maximum capacity of ≈4 CO_2 molecules per formula unit at 288 K, which decreases down to ≈3 CO_2 molecules/formula unit when increasing the temperature up to 318 K.[28,33]

In any case, it should be highlighted that even if the volume expansion at the phase transition increases the endothermic barocaloric effects, it also maximizes the CO_2 adsorption and, in turn, the adsorption exothermal thermal changes. Therefore, these caloric effects show a similar mechanism than in the case of MIL-53(Al),[29] even if MOF-508b combines subnetwork displacements with breathing transitions, and can be catalogued as breathing-caloric-like effects.

2.4. Analysis of Caloric Parameters for Refrigeration Applications

The here reported breathing-caloric-like effects of MOF-508b show characteristics typical of vapor compression (refrigerant fluid compression) and barocaloric refrigeration (pressure-induced solid-solid transitions) combined with gas adsorption.

For that reason, we compare the caloric parameters of MOF-508b with some of the best commercial refrigerants used in vapor compression,[30] as well as some of the best barocaloric materials[12–18] recently reported.

As can be observed in **Figure 3a**, the MOF-508b exhibits thermal changes (isothermal entropy changes, ΔS) superior to most barocaloric materials[12–18] and also to the previously reported breathing-caloric MIL-53(Al),[29] and in the range of refrigerant gases. Further, this material can operate under pressures as small as 26 bar and in environmental temperatures and climates from 273–333 K (Figure 3b), which matches the commercial requirements of commercial refrigeration gases.

It should also be noted that MOF-508b operates at significantly lower pressures than stand-alone CO_2 and even overcomes the operating limit of 31 °C related to CO_2 critical point.

Compared with MIL-53(Al), MOF-508b does not require thermal activation. However, MIL-53(Al) has been more studied and presents important advantages over MOF-508b, such as greener synthesis (using H_2O instead of DMF/EtOH as solvent) and already known scale-up conditions. Therefore, future efforts must be made to improve synthesis conditions in the less explored MOF-508b.

In the same line, recent studies present theoretical compression-driven adsorption heat pumps and refrigeration systems based on porous materials, such as active carbons or non-flexible MOFs.[35,36] These theoretical devices show COP as large as ≈5–6 under CO_2 pressures of 40–70 bar, which can be further improved using lower operating pressures, such as in the case of MOF-508b. Therefore, our findings also offer new candidates for performing theoretical modeling of heating and/or cooling devices.

2.5. Thermometry Device

In order to design and manufacture refrigeration devices, one of the most important thermodynamic parameters is the temperature change experienced by the material when the pressure is applied and/or removed. For this purpose, we have developed the first thermometry device that can evaluate such temperature changes under full hydrostatic pressurization (Figure 3c). This represents an important advantage with respect to previous thermometry devices for barocaloric materials, which only reaches quasi-hydrostatic pressure through the use of a uniaxial piston.[38–40]

In brief, the device is formed by a pressurization chamber, where the studied sample and a reference material (Al_2O_3) surround a thermocouple that monitors the temperature of both materials over time. Here, the CO_2 pressure inside the chamber is controlled by inlet and outlet valves, and it is recorded by a pressure transducer.

Figure 3d shows the adiabatic temperature change of our MOF-508b upon pressurization and depressurization, which exhibits values as large as $\Delta T \approx 30$ K under operating pressures of only 26 bar. Remarkably, this temperature change seems to remain invariable over time when cycling the material. Meanwhile, the Al_2O_3 reference, a well-known non-porous material,[41] presents a minimal temperature change of $\Delta T \approx 2$ K under the same conditions as MOF-508b. As can be observed in Figure 3d, both materials reach their peak temperatures instantaneously after pressurization and/or depressurization. It should be noted that the different transition kinetics in pressurization and depressurization, as previously observed by VP-DSC (Figure 1b), does not limit the pressurization rate of the thermometry device, which reaches the maximum pressure almost instantaneously (Figure 3d).

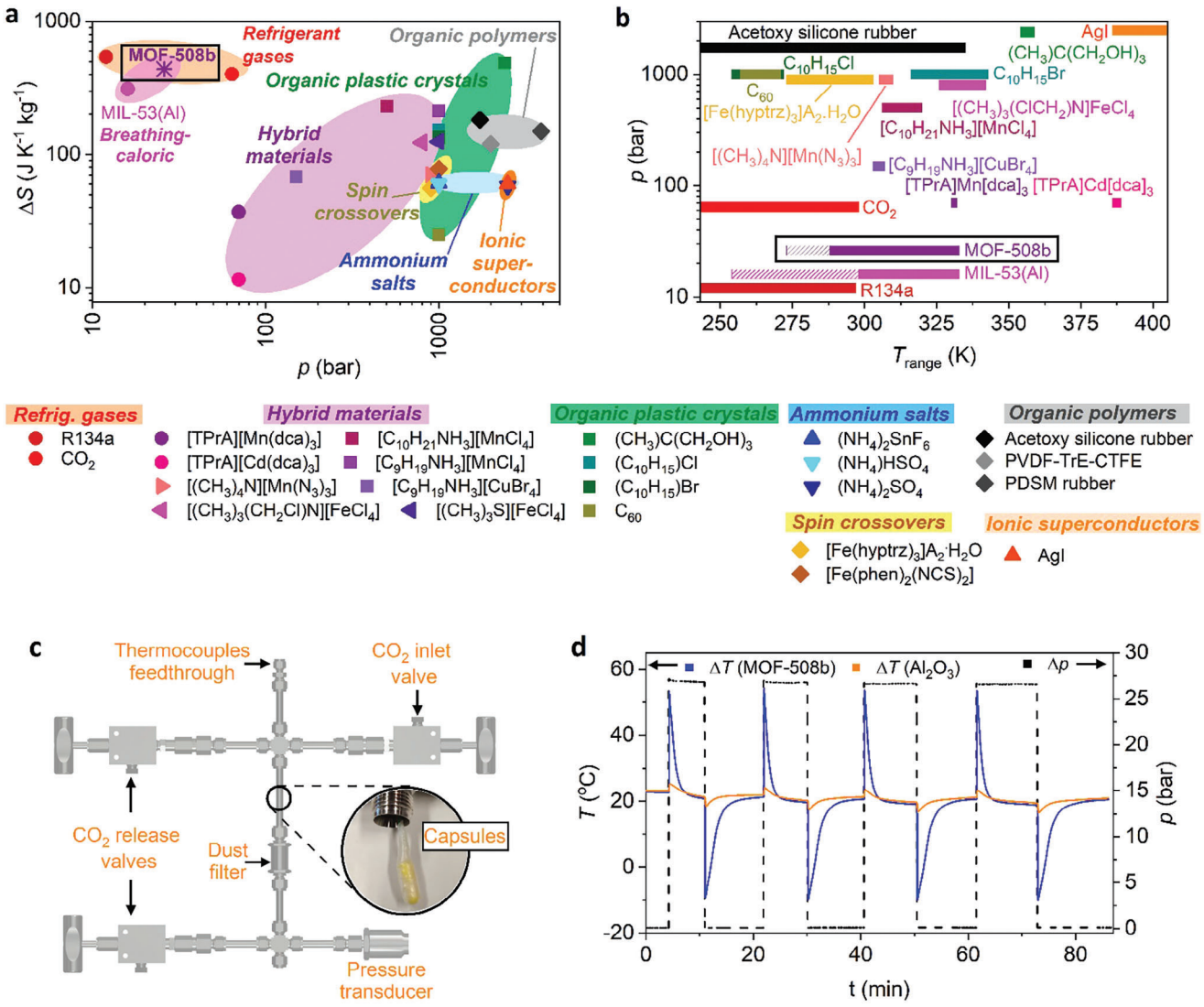

Figure 3. a,b) Main caloric parameters of MOF-508b in comparison with commercial refrigeration gases,[30] the so-far only known breathing-caloric material MIL-53(Al),[29] and a selection of the best reported barocaloric materials[12–18]: Isothermal entropy change versus operating pressure (a) and operating pressure versus operating temperature range –temperature span– (b). Note: black boxes indicate the values for MOF-508b observed in the present work. Shadowed areas represent the estimated operating temperature range according to reported isothermal adsorption analysis.[29,37] c) Thermometry device for studying barocaloric and breathing-caloric-like materials. The materials are inserted in pin-holed insulating capsules in the form of powders. d) Adiabatic temperature change observed for the MOF-508b compound under CO_2 pressurization and depressurization of 26 bar at room temperature. Note: the non-porous Al_2O_3 compound is used as blank material.

The main time limitation would be the thermalization back to ambient temperature, which currently requires 5–10 min because MOFs have very low thermal conductivities and the MOF-508b is inserted in a pin-holed insulating capsule and covered with a layer of another insulating polymer for maintaining adiabatic conditions. Therefore, the thermalization time and heat transfer can be easily improved in the future by using conductive materials for the capsules as well as by making composites of MOF-508b with thermal conductive additives.

For comparison purposes, it must be indicated that the reported quasi-hydrostatic devices have registered temperature changes as large as $\Delta T \approx 40$ K for organic polymers; although, under much larger applied pressures of 3900 bar, which is an important drawback for technological applications.[42] Meanwhile, when reducing the operating pressure down to 300 bar, the temperature change decreases down to $\Delta T \approx 2$ K.[39,40,42]

In the case of our studies on MOF-508b, with a $\Delta T \approx 30$ K at just 26 bar at room temperature (296 K, 23 °C), we are able to obtain, in a cyclic and reproducible manner over time, heating temperatures as large as 56 °C when pressurizing, and cooling temperatures as low as −10 °C when depressurizing (Figure 3d). These temperatures and operating pressure are already very adequate for many commercial applications, such as space heating, air-conditioning, and even food refrigeration and freezing, among others.

Interestingly, the device geometry allows not only to allocate pin-holed capsules but also to directly integrate the materials' powders inside the naked pipe to facilitate heat transfer. Further, this pipe-shaped design will also allow to connect several pipes in series to fabricate a heat exchange array for pre-commercial prototypes. Advantageously, similar to barocaloric materials (which are generally obtained as powders), MOFs can be integrated in devices in many different ways, such as in the shape of powders (contained by filters or membranes) to maximize surface exposure to CO_2 while allowing gas flow, or in the shape of pellets or even monoliths (to avoid such contention elements), which also opens the door to future studies about the conformation influence on the final breathing-caloric-like effects.

3. Conclusion

In this work, we have identified a very promising solid-state material for eco-friendly cooling and heating applications, the MOF-508b, which overcomes most of the major limitations of vapor compression gases (especially CO_2), adsorption refrigerants, barocaloric materials, and the only reported breathing-caloric material, the MIL-53(Al).

Differently from MIL-53(Al), the MOF-508b exhibits not one but two pressure-induced phase transitions, giving rise to thermal changes as large as $\Delta H \approx 130.6$ kJ kg^{-1} and $\Delta S \approx 438.0$ J K^{-1} kg^{-1} (40% superior to those of MIL-53(Al)). These thermal changes are related to the combination of volume and structural changes of the solid transitions with CO_2 adsorption/desorption processes.

Remarkably, the thermal changes are in the range of vapor compression refrigerant gases and largely surpass those exhibited by emerging barocaloric materials. In addition, it operates at much lower pressures than barocaloric materials and even than stand-alone CO_2 refrigerant, decreasing the operating pressure from $p \geq 1000$ bar (barocalorics) or $p \geq 70$–150 bar (CO_2) down to $p \leq 26$ bar. Moreover, MOF-508b expands the operating temperature range from 273 to 333 K, which is much larger than any other barocaloric and also overcomes the limitation of stand-alone CO_2 to operate in warm climates due to its critical point (304 K). Even more, MOF-508b avoids the thermal regeneration generally required for adsorption refrigerants and even the thermal activation needed for the breathing-caloric MIL-53(Al). MOF-508b also presents much lower volume changes ($\Delta V \leq 14\%$) than MIL-53(Al) ($\Delta V \approx 40\%$), which would minimize mechanical strains and fatigue in the designed heating and cooling devices.

In addition, from the technological integration point of view, we introduce the first thermometry device for evaluating the pressure-induced temperature changes in breathing-caloric (and also in barocaloric)-like materials under hydrostatic gas pressurization. This device allows us to demonstrate that, at room temperature and under the pressure application of only 26 bar, MOF-508b exhibits heating temperatures up to 56 °C and cooling temperatures down to −10 °C, which are already useful for space heating, air-conditioning, and food refrigeration and freezing.

Therefore, these results strengthen the potentiality of the emerging breathing-caloric-like materials to empower CO_2 eco-friendly heating and cooling and provide important insights to accelerate the development of more advanced prototypes using solid-state materials. In turn, this work opens the door toward further studies for addressing important aspects of these new technology, such as deepening in the understanding and controlling kinetics and the thermal contributions of both solid–solid transition and adsorption/desorption processes to enhance the performance of breathing-caloric-like materials.

4. Experimental Section

Synthesis: The MOF-508b material was obtained by adapting the method reported by M. Bonneau et al.[37] Terephthalic acid [H_2bdc] (Merck 98%), 4,4′-Bipyridine [bpy] (Merck 98%), $Zn(NO_3)_2{\cdot}6H_2O$ (Merck 99%), *N*,*N*-Dimethylformamide [DMF] (Fischer Scientific ≥99.8%), and absolute ethanol [EtOH] (Scharlab) were used without further purification. A mixture of H_2bdc (0.498 g, 3 mmol) in DMF (20 mL), of $Zn(NO_3)_2{\cdot}6H_2O$ (0.892 g, 3 mmol) in EtOH (15 mL), and of bpy (0.234 g, 1.5 mmol) in DMF (7.5 mL) was stirred at 373 K during 24 h using a reflux synthesis setup. A white precipitate was collected by centrifugation, washed with DMF (2 × 20 mL), and dried under vacuum at $T = 393$ K for 24 h to finally obtain the desired MOF-508b compound.

Powder X-Ray Diffraction (PXRD): The obtained material was characterized by powder X-ray diffraction (PXRD) using a Siemens D-5000 diffractometer with Cu(Kα) radiation at room temperature. The obtained patterns were compared with those simulated from reported single-crystal XRD.[33]

The structural evolution of the material over pressure at different temperatures was studied by synchrotron powder X-ray diffraction (SPXRD) using a wavelength of $\lambda = 0.71073$ Å. These studies were carried out at the BM01 Swiss Norwegian Beamline (SNBL) of the European Synchrotron Radiation Facility (ESRF).[43] For those experiments, 0.5 mm diameter quartz capillaries were filled with MOF-508b powder and measured in situ at isothermal conditions of 298, 303, and 320 K under CO_2 atmosphere between vacuum and up to 35 bar. The temperature was controlled with an Oxford Cryostream 700+, and diffraction data were collected with a Pilatus 2 M detector. The recorded 2D patterns were integrated into a 1D powder profile and fitted using the Le Bail method. The diffraction patterns were refined using the GSAS-II software.[44]

Scanning Electron Microscopy (SEM): The particle size and morphology of the MOF-508b compound were studied by scanning electron microscopy using a Jeol JSM-6400 microscope with a 5 kV voltage. The sample was previously sputtered with a thin layer of Pt/Pd. The particle size was calculated using 200 particles randomly selected.

Isothermal Adsorption Analysis: N_2 sorption isotherm was measured at 77 K using an ASAP 2020 Micrometrics instrument. The sample was previously degassed at 393 K under vacuum for 12 h. The overall specific surface area was estimated by fitting the N_2 sorption isotherm to the BET and Langmuir models.

Variable-Pressure Differential Scanning Calorimetry (VP-DSC): The pressure-induced caloric response of the MOF-508b compound was studied by variable-pressure differential scanning calorimetry (VP-DSC) in TA Instruments pressure-cell mounted on a Q2000 MDSC (modulated differential scanning calorimeter), which was bespoke upgraded to control the CO_2 pressure ramps, as described in the authors' previous work.[29] Here, the CO_2 pressure was controlled by a Bronkhorst EL-PRESS P-802CV in the inlet and by a Bronkhorst EL-FLOW Select F-201CV flux in the outlet. In all experiments, ≈5 mg aliquots of powdered samples were used. The calorimetric measurements were performed under pressurization/depressurization ramps of CO_2 at different rates (0.9–2.5 bar min^{-1}) and under different isothermal conditions (288–333 K), maintaining a constant gas flux of 50 mL min^{-1}. The calorimeter was previously calibrated according to the manufacturer recommendations and verified with an indium reference. The baseline was corrected by using empty pans as blank samples under CO_2 pressurization and depressurization. The thermal changes were calculated by

integrating the heat flow, as reported elsewhere,[45] taking into account the corrections and calibrations described above, following Equation (1):

$$|\Delta S|_{0\rightarrow p} = \frac{1}{T}|\Delta H|_{0\rightarrow p} = \frac{1}{T}\int_0^p \left(\frac{dQ}{dp}\right) dp \quad (1)$$

where (dQ/dp) is the heat flow curve as a function of pressure, after subtracted the heat flow of the CO_2 pressurization on the empty pan, 0 and p are the initial and final pressures, and T is temperature at each isothermal measurement.

In addition, and for comparison purposes, a point-by-point calorimetric analysis (following reported methods[29,46]) was performed by increasing the CO_2 pressure in steps of 0.5 bar from 1.5 to 26 bar under isothermal conditions at ≈298 K and registering the heat flow.

Thermogravimetric Analysis (TGA): The thermal stability of MOF-508b was studied by thermogravimetric analysis (TGA) using a NETZSCH STA 449F3 Jupiter equipment. Around 15 mg of a MOF-508b powder sample in an alumina crucible was heated from room temperature up to 1266 K with a rate of 10 K min^{-1}, and under a 100 mL min^{-1} flow of dry nitrogen.

Fabrication of Thermometry Device: A device for thermometry analysis of barocaloric and breathing-caloric-like materials was devised following the design of reported high-pressure reactors for continuous flow hydrothermal synthesis.[47] The device consisted of a stainless steel central pipe that could allocate the samples and that was connected to two union crosses, which were subsequently connected to a thermocouples' feedthrough, one pressure transducer, one gas inlet-valve, and two gas outlet-valves.

Around 100 mg of each powdered sample was embedded into pin-holed insulating capsules that were wrapped into insulating polymeric film to maintain adiabatic conditions. While several capsules could be mounted and measured at the same time, the response of MOF-508b and Al_2O_3 (this latter used as blank material) was simultaneously studied. Type K thermocouples were embedded inside the materials' powders of each capsule to monitor the temperature changes. The temperature was registered using a calibrated picolog TC-8 data logger. Meanwhile, the pressure was registered using a Wika CPT2500 pressure transducer. The pressure was increased from 1 to 26 bar by using a CO_2 cylinder connected to the inlet-valve. The depressurization was done using the bottom outlet-valve. Meanwhile, the upper release valve was placed as a secondary outlet valve in case the bottom one got stuck with powder leaks. For the same purpose, a safety dust filter was installed before the bottom release valve to contain any possible leak. This dust filter would be useful in future studies where the whole central pipe would be directly filled with powders without using insulating pin-holed capsules.

All the high-pressure pipes (3/8″), valves, and connections were purchased from Swagelok. The device size was ≈60 cm in width and 40 cm in height with a total inner volume of ≈50 cm^3.

Supporting Information

Supporting Information is available from the Wiley Online Library or from the author.

Acknowledgements

The authors are thankful for financial support from the grant PID2021-122532OB-I00 funded by MCIN/AEI/10.13039/501100011033 and by ERDF A way of making Europe, the project PDC2021-121076-I00 funded by MCIN/AEI/10.13039/ 501100011033 and by the European Union Next GenerationEU/PRTR and the project ED431C 2022/39 funded by Xunta de Galicia. This publication is part of the grant RYC2021-033040-I, funded by MCIN/AEI/10.13039/ 501100011033 and from the European Union «NextGenerationEU»/PRTR» and granted to J.M.B.-G. This researcher is also grateful for the support received by UDC-Inditex InTalent Programme. J.G.-B. acknowledges Xunta de Galicia for Predoctoral Fellowships. The authors thank ESRF for the award of beam time (MA-5145 and A01-2-1291 on BM01). Funding for open access publication granted by Universidade da Coruña/CISUG.

Conflict of Interest

The authors declare no conflict of interest.

Author Contributions

M.G. and J.G.-B. contributed equally to this work. S.R-H., M.S.-A, M.A.S.-R., and J.M.B.-G. conceived the project. M.G., J.G.-B., S.C.-G., M.S.-A., M.A.S.-R., and J.M.B.-G. wrote the manuscript. All authors were involved in the experimental design and work and contributed to materials and analysis tools, to the results discussion, and to the manuscript revision. M.A.S.-R. and J.M.B.-G. directed and supervised this project.

Data Availability Statement

The data that support the findings of this study are available from the corresponding author upon reasonable request.

Keywords

barocaloric, breathing-caloric, metal–organic frameworks, thermomaterials, thermometry

Received: October 10, 2023
Revised: November 29, 2023
Published online:

[1] *Policy Support for Heating and Cooling Decarbonization*, European Commission, **2022**. https://data.europa.eu/doi/10.2833/977806 (accessed: November 2023).
[2] United Nations Sustainable Development Goals, https://sdgs.un.org/goals (accessed: November 2023).
[3] D. Coulomb, J. L. Dupont, A. Pichard, in *The Role of Refrigeration in the Global Economy, 29th Note on Refrigeration Technologies*, International Institute of Refrigeration, **2015**.
[4] *Renewables 2019: Analysis Forecast to 2024*, International Energy Agency, https://www.iea.org/reports/renewables-2019 (accessed: November 2023).
[5] M. Isaac, D. P. Van Vuuren, *Energy Policy* **2009**, *37*, 507.
[6] *Carbon Capture, Storage and Utilization*, European Commission, https://energy.ec.europa.eu/topics/oil-gas-and-coal/carbon-capture-storage-and-utilisation_en (accessed:November 2023).
[7] S. Dilshad, A. R. Kalair, N. Khan, *Int. J. Energy Res.* **2020**, *44*, 1408.
[8] *Commercial CO_2 Refrigeration Systems: Guide for Subcritical and Transcritical CO_2 Applications*, Emerson Climate Technologies, **2015**.
[9] A. N. Shmroukh, A. H. H. Ali, S. Ookawara, *Renewable Sustainable Energy Rev.* **2015**, *50*, 445.
[10] F. Shabir, M. Sultan, T. Miyazaki, B. B. Saha, A. Askalany, I. Ali, Y. Zhou, R. Ahmad, R. R. Shamshiri, *Renewable Sustainable Energy Rev.* **2020**, *119*, 109630.
[11] H. Demir, M. Mobedi, S. Ülkü, *Renewable Sustainable Energy Rev.* **2008**, *12*, 2381.
[12] P. Lloveras, J.-L. Tamarit, *MRS Energy Sustainability* **2021**, *8*, 3.
[13] J. M. Bermúdez-García, M. Sánchez-Andújar, S. Castro-García, J. López-Beceiro, R. Artiaga, M. A. Señarís-Rodríguez, *Nat. Commun.* **2017**, *8*, 15715.

[14] B. Li, Y. Kawakita, S. Ohira-Kawamura, T. Sugahara, H. Wang, J. Wang, Y. Chen, S. I. Kawaguchi, S. Kawaguchi, K. Ohara, K. Li, D. Yu, R. Mole, T. Hattori, T. Kikuchi, S. ichiro Yano, Z. Zhang, Z. Zhang, W. Ren, S. Lin, O. Sakata, K. Nakajima, Z. Zhang, *Nature* **2019**, *567*, 506.
[15] P. Lloveras, A. Aznar, M. Barrio, P. Negrier, C. Popescu, A. Planes, L. Mañosa, E. Stern-Taulats, A. Avramenko, N. D. Mathur, X. Moya, J.-L. Tamarit, *Nat. Commun.* **2019**, *10*, 1803.
[16] J. Li, M. Barrio, D. J. Dunstan, R. Dixey, X. Lou, J.-L. Tamarit, A. E. Phillips, P. Lloveras, *Adv. Funct. Mater.* **2021**, *31*, 2105154.
[17] J. Seo, R. D. Mcgillicuddy, A. H. Slavney, S. Zhang, R. Ukani, A. A. Yakovenko, S.-L. Zheng, J. A. Mason, *Nat. Commun.* **2022**, *13*, 2536.
[18] J. Seo, J. D. Braun, V. M. Dev, J. A. Mason, *J. Am. Chem. Soc.* **2022**, *144*, 6493.
[19] X. Moya, I. M. Ilevbare in *Materials for the Energy Transition roadmap: Caloric Energy Conversion Materials*, Henry Royce Institute, **2020**, https://www.royce.ac.uk/content/uploads/2021/10/M4ET-Caloric-Energy-Conversion-Materials-roadmap.pdf (accessed: November 2023).
[20] K. Barthelet, J. Marrot, D. Riou, G. Férey, *Angew. Chem., Int. Ed.* **2002**, *41*, 281.
[21] S. Bourrelly, P. L. Llewellyn, C. Serre, F. Millange, T. Loiseau, G. Férey, *J. Am. Chem. Soc.* **2005**, *127*, 13519.
[22] D. Boldrin, *Appl. Phys. Lett.* **2021**, *118*, 170502.
[23] P. Iacomi, F. Alabarse, R. Appleyard, T. Lemaire, C. Thessieu, S. Wang, C. Serre, G. Maurin, P. G. Yot, *Angew. Chem., Int. Ed.* **2022**, *134*, e202201924.
[24] H.-C. J. Zhou, S. Kitagawa, *Chem. Soc. Rev.* **2014**, *43*, 5415.
[25] A. Schneemann, V. Bon, I. Schwedler, I. Senkovska, S. Kaskel, R. A. Fischer, *Chem. Soc. Rev.* **2014**, *43*, 6062.
[26] G. Férey, C. Serre, *Chem. Soc. Rev.* **2009**, *38*, 1380.
[27] J. A. Mason, J. Oktawiec, M. K. Taylor, M. R. Hudson, J. Rodriguez, J. E. Bachman, M. I. Gonzalez, A. Cervellino, A. Guagliardi, C. M. Brown, P. L. Llewellyn, N. Masciocchi, J. R. Long, *Nature* **2015**, *527*, 357.
[28] W. K. Feldmann, C. Esterhuysen, L. J. Barbour, *ChemSusChem* **2020**, *13*, 5220.
[29] J. García-Ben, J. López-Beceiro, R. Artiaga, J. Salgado-Beceiro, I. Delgado-Ferreiro, Y. V. Kolen'ko, S. Castro-García, M. A. Señarís-Rodríguez, M. Sánchez-Andújar, J. M. Bermúdez-García, *Chem. Mater.* **2022**, *34*, 3323.
[30] *Thermophysical Properties of Refrigerants*, *ASHRAE Handbook*: *Fundamentals*, ASHRAE, **2009**.
[31] B. Chen, C. Liang, J. Yang, D. S. Contreras, Y. L. Clancy, E. B. Lobkovsky, O. M. Yaghi, S. Dai, *Angew. Chem., Int. Ed.* **2006**, *45*, 1390.
[32] L. Bastin, P. S. Bárcia, E. J. Hurtado, J. A. C. Silva, A. E. Rodrigues, B. Chen, *J. Phys. Chem. C* **2008**, *112*, 1575.
[33] P. M. Bhatt, E. Batisai, V. J. Smith, L. J. Barbour, *Chem. Commun.* **2016**, *52*, 11374.
[34] A. V. Neimark, F.-X. Coudert, C. Triguero, A. Boutin, A. H. Fuchs, I. Beurroies, R. Denoyel, *Langmuir* **2011**, *27*, 4734.
[35] G. Kumar, S. Sahoo, *J. Inst. Eng. (India): Series C* **2023**, *104*, 853.
[36] J. A. Shamim, G. Auti, H. Kimura, S. Fei, W.-L. Hsu, H. Daiguji, A. Majumdar, *Cell Rep.* **2022**, *3*, 101131.
[37] M. Bonneau, C. Lavenn, J.-J. Zheng, A. Legrand, T. Ogawa, K. Sugimoto, F.-X. Coudert, R. Reau, S. Sakaki, K.-I. Otake, S. Kitagawa, *Nat. Chem.* **2022**, *14*, 816.
[38] N. M. Bom, E. O. Usuda, G. M. Guimarães, A. A. Coelho, A. M. G. Carvalho, *Rev. Sci. Instrum.* **2017**, *88*, 5.
[39] J. Garcia-Ben, I. Delgado-Ferreiro, J. Salgado-Beceiro, J. M. Bermudez-Garcia, *Materials* **2021**, *14*, 5947.
[40] N. M. Bom, W. Imamura, E. O. Usuda, L. S. Paixão, A. M. G. Carvalho, *ACS Macro Lett.* **2018**, *7*, 31.
[41] L. E. C. De Torre, E. S. Flores, J. L. Llanos, E. J. Bottani, *Langmuir* **1995**, *11*, 4742.
[42] W. Imamura, É. O. Usuda, L. S. Paixão, N. M. Bom, A. M. Gomes, A. M. G. Carvalho, *Chin. J. Polym. Sci.* **2020**, *38*, 999.
[43] V. Dyadkin, P. Pattison, V. Dmitriev, D. Chernyshov, *J. Synchrotron Radiat.* **2016**, *23*, 825.
[44] B. H. Toby, R. B. Von Dreele, *J. Appl. Crystallogr.* **2013**, *46*, 544.
[45] *Barocaloric Effects in the Solid State: Materials and Methods*, IOP Publishing, **2023**.
[46] P. L. Llewellyn, G. Maurin, *C. R. Chim.* **2005**, *8*, 283.
[47] J. Sierra-Pallares, T. Huddle, J. García-Serna, E. Alonso, F. Mato, I. Shvets, O. Luebben, M. J. Cocero, E. Lester, *Nano Res.* **2016**, *9*, 3377.